Theory of space charge limited regime of thermionic energy converter with negative electron affinity emitter

Joshua Ryan Smith, Griff L. Bilbro and Robert J. Nemanich

Citation: Journal of Vacuum Science & Technology B: Microelectronics and Nanometer Structures Processing, Measurement, and Phenomena **27**, 1132 (2009); doi: 10.1116/1.3125282

View online: https://doi.org/10.1116/1.3125282

View Table of Contents: https://avs.scitation.org/toc/jvn/27/3

Published by the American Institute of Physics

Theory of space charge limited regime of thermionic energy converter with negative electron affinity emitter

Joshua Ryan Smith[a)]
Department of Materials Science and Engineering, Carnegie Mellon University, Pittsburgh, Pennsylvania 15213-3890

Griff L. Bilbro
Department of Electrical and Computer Engineering, North Carolina State University, Raleigh, North Carolina 27695-7911

Robert J. Nemanich
Department of Physics, Arizona State University, Tempe, Arizona 85287-1504

(Received 8 August 2008; accepted 3 April 2009; published 15 May 2009)

A theory of the space charge limited output current regime of a vacuum thermionic energy conversion device (TEC) employing a negative electron affinity (NEA) diamond emitter electrode is derived. The theory is developed by assuming that the electrons behave as a collisionless gas and self-consistently solving Vlaslov's equation and Poisson's equation. Special cases of the theory are addressed. Calculations are performed to model a TEC with a nitrogen doped diamond emitter material under various conditions. It is shown that the NEA material outperforms a similar positive electron affinity material in terms of output power and efficiency because the NEA lowers the electrostatic boundary condition at the emitter and therefore mitigates the negative space charge effect. © *2009 American Vacuum Society.* [DOI: 10.1116/1.3125282]

I. INTRODUCTION

In recent years, interest has grown in efficient energy conversion technology as people worldwide investigate the so-called green technology. In this article, the performance of a highly efficient direct energy conversion device known as a vacuum thermionic energy converter (TEC) is modeled and characterized. The TEC configuration under consideration employs a hydrogen terminated, doped diamond material as the emitter electrode which allows the device to operate at a lower emitter temperature and avoid performance-reducing space charge effects. This report builds on our previous work[1] which established one bound of the space charge limited regime by expanding the model to predict the entire space charge mode of operation.

A vacuum thermionic energy conversion device is a two-terminal vacuum diode configured to convert heat directly to electrical work via thermionic emission. First proposed by Schlichter[2] and schematically depicted in Fig. 1, the TEC operates as follows: the emitter electrode is held at a higher temperature than the collector electrode. Electrons are thermionically emitted and travel across the evacuated interelectrode space. The electrons arrive at the collector electrode and are absorbed. They travel out the vacuum container through an electrical lead and do useful work in an external load. The electrons travel through another lead back to the emitter and thus complete the circuit.

Vacuum TECs have the potential to efficiently generate electrical work because heat transport across the device is chiefly restricted to two mechanisms: thermionic electrons from the emitter to the collector and Stefan–Boltzmann radiation from both the collector and the emitter. Due to the vacuum gap, phonons do not contribute to heat transport, in contrast to a thermoelectric device. The resulting advantage in efficiency was recognized early in the development of thermionic technology.[3]

The physical limitations of vacuum thermionic devices hampered the development of the technology. First, emitter materials were refractory metals with relatively large work functions of 4 or 5 eV. These high work function materials required high operating temperatures ($\geqslant$1500 K) to achieve appreciable output power which relegated TECs to niche applications. To lower the high operating temperatures, the materials required low work function coatings which were unstable. The decisive limitation resulted from the negative space charge effect. This phenomenon can be explained as follows: as electrons are emitted into the evacuated interelectrode space, a net negative charge develops which presents an extra electrostatic barrier to the electrons. The less energetic electrons cannot surmount this additional electrostatic barrier, thereby limiting the output current and output power of the device. To overcome this space charge limitation, early investigators determined that the interelectrode space of the device had to be below 1 μm.[4,5] This constraint rendered vacuum TECs technologically unfeasible and subsequent research focused on vapor thermionic devices. Here we use the terms "space charge" and "space charge *effect*" where the former denotes the presence of electrons in the interelectrode space, while the latter refers to the condition these electrons impose on the output current of the TEC.

Diamond materials exhibit properties that may provide solutions to both of these historical limitations of vacuum TECs. A key feature of hydrogen terminated diamond for this application is the negative electron affinity (NEA): the

[a)]Electronic addresses: josnuasm@andrew.cmu.edu and jrsmith@cmu.edu

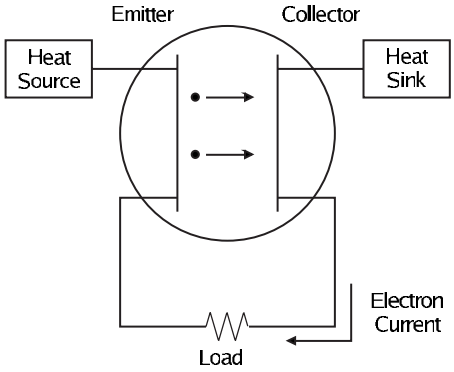

FIG. 1. Schematic of vacuum thermionic energy conversion device.

vacuum level of the surface falls below the conduction band minimum of the material. Many surface orientations of diamond have been observed to acquire a NEA when hydrogen terminated, including the (100), (110), (111), and polycrystalline surfaces.[6–12] Moreover, in diamond the donor level of nitrogen lies roughly 1.7 eV below the conduction band minimum,[13] and the donor level of phosphorus has been reported to lie 0.6 eV below the conduction band minimum.[14,15] According to ultraviolet photoemission spectroscopy, thermionic emission spectroscopy,[16] and temperature limited thermionic emission measurements[17] performed in our laboratory, the thermionic barrier height of nitrogen doped diamond approaches 1.4 eV at temperatures of 300–500 °C. This low emission barrier allows for sub-1000 K operating temperature of the TEC.

Our previous study has shown that the negative electron affinity can mitigate the negative space charge effect in a vacuum TEC. The NEA property lowers the electrostatic boundary condition just outside the emitter electrode, and by solving Poisson's equation and Vlasov's equation it was shown the additional space charge barrier was lowered in the interelectrode space. Put another way, the lowest energy electrons which are thermionically emitted from a NEA surface will leave the surface with significant kinetic energy. In essence, the NEA acts as a filter to eliminate the slowest electrons which are most affected by the negative space charge.[1,18] This article provides a detailed theoretical description of the entire space charge limited mode of the output current characteristic of a vacuum TEC employing a NEA diamond emitter material. It goes beyond our previous study by providing a prescription to calculate the output current characteristic for the whole of the space charge limited regime; our previous work deals only with the calculation of one boundary of this regime. The theory is applied to a thermionic device featuring a nitrogen doped diamond emitter electrode. It is shown that the NEA property of the H-terminated diamond mitigates the negative space charge effect, consistent with previous results.[1,18] Additionally, the theory predicts cases where the space charge limited mode can be avoided altogether. Several mathematical details of the theory are addressed as well.

Since this report focuses on the electron transport across the interelectrode space, simplifying assumptions about some surface phenomena were made. As was previously stated, the NEA is taken to lower the electrostatic boundary condition at the emitter. Phenomena such as surface band bending and potential lowering due to image charge effects will affect the thermionic emission from the emitter, but should not essentially alter the results of this investigation.

II. THEORY

The goal of this theoretical development is to characterize the space charge limited regime of the output current characteristic, specifically for the case of a TEC with a NEA material as the emitter electrode. Theoretical characterizations of TECs have historically been concerned with the transport of electrons across the interelectrode space; this theory, therefore, will address the same. The development presented here will follow the same strategy as previous studies by considering the electrons in the interelectrode space as a collisionless gas and self-consistently solving Vlaslov's equation and Poisson's equation.[5,19–21] Here electron current is taken to be positive.

Typically, for a set of device parameters, there exists a region of the output current characteristic for which the output current is space charge limited. In the case of a NEA emitter, this region is bounded by the virtual saturation point[1] and the critical point, terms for conditions of device operation which will be defined shortly. To qualitatively understand the physics of the situation, it is useful to consider a so-called motive diagram, which is similar to a band diagram in a semiconductor device. The motive in the interelectrode space is equal to the electrostatic potential times $-e$, where e is the fundamental charge. Throughout this article we denote the motive by ψ. Figure 2 graphically illustrates several features of this theory: the figure shows an output current characteristic of a NEA TEC, along with corresponding motive diagrams for key points on each. The corresponding picture of a conventional TEC can be found on pp. 94 and 96 of Hatsopoulos and Gyftopoulos.[5] It is noted that the output current characteristic in Fig. 2(f) is not single valued. A discussion of this phenomenon is given in part C of the appendix where it is shown that the physically observed current will be the current associated with the minimum output power. We have chosen to leave the non-single valued parts of the output characteristics in the graphs but we quote only physically realizable values of output quantities in the text of this report, denoted where necessary by an asterisk.

This development follows the theory of electron transport through a vacuum TEC described by Hatsopoulos and Gyftopoulos,[19] especially their definition of a surface and points just outside the surface.[19] This idea is presented here for clarity: the motive is continuous from points inside the material to points outside the material. Near the surface of the material, the motive varies significantly with respect to position: the variation occurs over the distance of a few tens of nanometers. "A point just outside the surface" is where the motive no longer varies so dramatically. Since the interfacial region of the surface of the material is small relative to the dimensions of the device, we assume that the surface of the

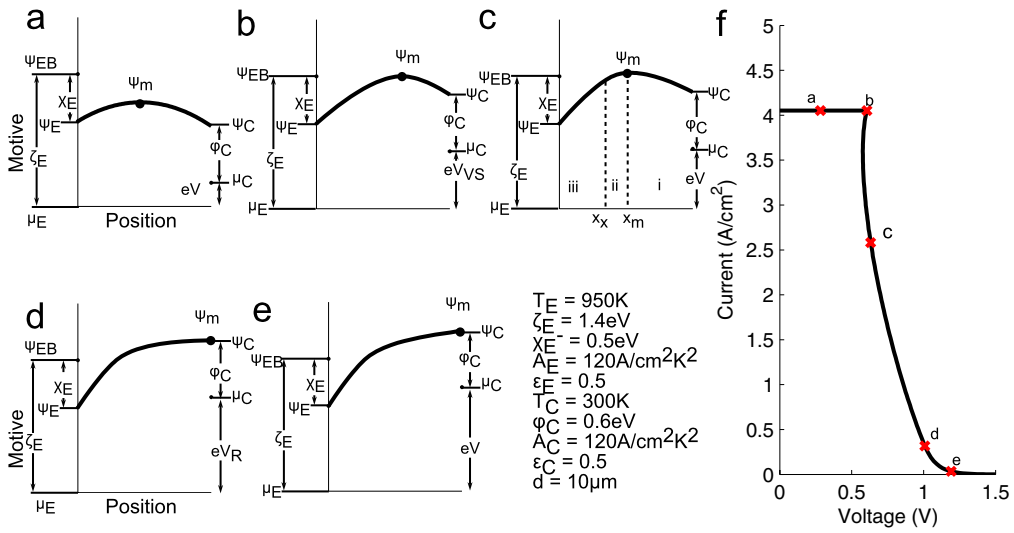

FIG. 2. (Color online) (a) Typical motive diagram corresponding to the accelerating range of voltages. (b) Motive diagram corresponding to the virtual saturation point. (c) Typical motive diagram of the space charge limited mode. (d) Motive diagram of the critical point. (e) Typical motive diagram corresponding to the retarding range of voltages. (f) Output current characteristic showing distinct regions and special points.

material occurs at a singular position and that the vacuum level of the material defines the electrostatic boundary condition for the interelectrode space.

In Fig. 2, the emitter and collector are held at temperatures T_E and T_C, respectively. Both have Richardson's constants of A_E and A_C, respectively. It should be noted that Richardson's constant is considered as a material property as opposed to a constant. The emission barrier height of the emitter is ζ_E, the value of the negative electron affinity is χ_E^-, and the work function is ϕ_E. The emitter's Fermi level is denoted by μ_E, its vacuum level is denoted by ψ_E, and its conduction band minimum is given by ψ_{EB}. Except for ζ, the collector has the same attributes as the emitter and are distinguished by a subscript "C." Additionally, the collector is at some voltage V with respect to the emitter as determined by the load and the output current flowing through the device. The maximum motive is denoted by ψ_m.

Figure 2(a), shows the motive which corresponds to the accelerating regime. Here, the maximum motive occurs below the conduction band minimum and therefore all electrons emitted from the emitter travel unimpeded to the collector. The output current is equal to the emitter saturation current J_{ES} which is given by Richardson's equation. There exists a condition, designated the virtual saturation point, such that the maximum motive occurs coincident with the conduction band minimum. The virtual saturation condition bounds the space charge limited regime, and the motive is shown in Fig. 2(b). The adjective "virtual" was chosen to distinguish this case from the saturation point of a conventional TEC because the virtual saturation point occurs in the interelectrode space as opposed to immediately outside the emitter. We have previously reported a theoretical description of the virtual saturation point.[1]

The space charge limited mode is defined as the conditions such that the maximum motive occurs within the interelectrode space and presents an extra barrier over which electrons must pass to reach the collector. The motive diagram shown in Fig. 2(c) displays this condition. In this situation, the maximum motive occurs at a position x_m, and the motive crosses below the conduction band minimum at some position x_x. Here, the interelectrode space is partitioned into three regions: (i) $x > x_m$, (ii) $x_x < x < x_m$, and (iii) $x < x_x$. At the critical point, the maximum motive occurs immediately outside the collector. The critical point condition bounds the space charge regime and the motive diagram is shown in Fig. 2(d). For voltages above the critical point voltage, the collector vacuum level defines the maximum motive and the TEC is operating in the so-called retarding mode. The output current is given by $J = AT_E^2 \exp[-(\phi_C + eV)/kT_E]$ and the motive is easily determined. Figure 2(e) depicts the motive diagram.

Our strategy to calculate the space charge limited output current characteristic is as follows: First, the current and voltage corresponding to the virtual saturation point are determined. Next, the current and voltage corresponding to the critical point are calculated. Finally, using the virtual saturation point and critical point as the bounds, the values of current and voltage for the space charge limited regime are determined. Each of these steps follows a similar procedure: calculate the electron distribution function $f(x, v_e)$ in the interelectrode space, calculate the electron number density $n_e(x)$, then calculate a dimensionless Poisson's equation, and finally solve it numerically. An algorithm is developed which allows the theory to be implemented as a computer program.

A. Critical point

In the case of collisionless electrons, Vlaslov's equation can be solved to determine the distribution function of electrons[22] which is given by Eq. (1),

$$f(x,v_e) = 2n_e(x_m)\left(\frac{m_e}{2\pi kT_E}\right)^{3/2} \exp\left(\frac{\psi_m - \psi}{kT_E} - \frac{m_e v_e^2}{2kT_E}\right), \quad (1)$$

where x_m is the location of the maximum motive, $n_e(x_m)$ is the number density of electrons at x_m, ψ_m is the maximum motive. $\psi(x)$ is the value of the motive at point x, m_e is the electron mass, k is Boltzmann's constant, and $v_e \equiv (v_{ex}^2 + v_{ey}^2 + v_{ez}^2)^{1/2}$ is the magnitude of the velocity at a point in space.

At x_m, the electron distribution function is half-Maxwellian; i.e., for positive values of x-velocity the distribution is Maxwellian, otherwise the distribution is zero. Following Langmuir,[22] this fact can be exploited to construct the distribution function at all points in the interelectrode space. Consider the region i as shown in Fig. 2(c) Electrons in this region have been emitted from the emitter and have traveled over the space charge barrier. At a point in this region, the slowest electrons have a kinetic energy of $\psi_m - \psi$. Solving for the value of x-velocity, one can obtain a lower bound on electron velocity in this region, indicated by the unit step function, $u(v_e)$, for the region in Eq. (2). For regions i and ii, this analysis yields step functions which are identical to previous investigations.[22] However, the NEA at the emitter surface induces the region iii which introduces a novel element to the theory. Electrons in region iii are moving in both x-directions: some have been emitted from the emitter and are traveling toward the collector, and some have been reflected by the space charge barrier and are returning to the emitter. The minimum kinetic energy of electrons moving toward the collector is defined by the conduction band minimum of the emitter and the value of the motive, yielding a minimum velocity in the x-direction of $v_{ex} = [2(\psi_{EB} - \psi)/m_e]^{1/2}$, where ψ_{EB} defines the conduction band minimum. The kinetic energy of the electrons traveling toward the emitter is bounded above and below, and therefore the velocity of the electrons will be bounded above and below.

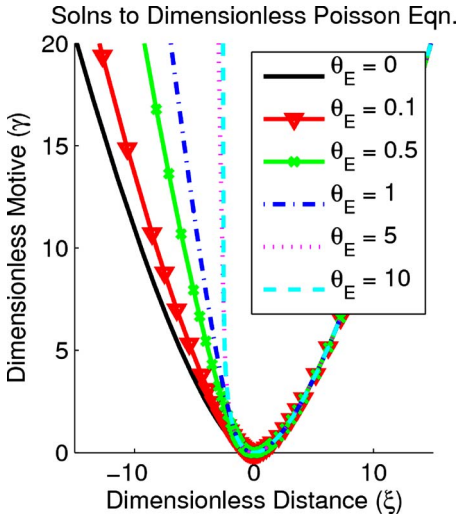

FIG. 3. (Color online) Solution to the dimensionless Poisson's equation for various values of θ_E. For positive values of ξ, the solution for each value of θ_E is the same.

The slowest electrons traveling toward the emitter are those which originated from the CBM; at point x_x, those electrons were reflected back toward the emitter and have a velocity of $v_{ex} = -[2(\psi_{EB} - \psi)/m_e]^{1/2}$. The fastest electrons traveling toward the emitter are the electrons which had slightly less energy than necessary to overcome the space charge barrier. These reflected electrons have a velocity of $v_{ex} = -[2(\psi_m - \psi)/m_e]^{1/2}$. Considering the limits on the velocity of the electrons in region iii, the electron distribution function can be expressed in terms of the unit step functions u. The fully assembled electron distribution function is given in Eq. (2). This equation describes the electrons within the interelectrode space and is therefore valid for values of position between the emitter ($x=0$) and collector ($x=d$),

$$f(x,v_e) = 2n_e(x_m)\left(\frac{m_e}{2\pi kT_E}\right)^{3/2} \exp\left[\frac{\psi_m - \psi}{kT_E} - \frac{m_e v_e^2}{2kT_E}\right] \times \begin{cases} u\left[v_{ex} - \left(2\dfrac{\psi_m - \psi}{m_e}\right)^{1/2}\right], & x > x_m \\ u\left[v_{ex} + \left(2\dfrac{\psi_m - \psi}{m_e}\right)^{1/2}\right], & x_x < x < x_m \\ u\left[v_{ex} + \left(2\dfrac{\psi_m - \psi}{m_e}\right)^{1/2}\right] - u\left[v_{ex} + \left(2\dfrac{\psi_{EB} - \psi}{m_e}\right)^{1/2}\right] + u\left[v_{ex} - \left(2\dfrac{\psi_{EB} - \psi}{m_e}\right)^{1/2}\right], & x < x_x. \end{cases} \quad (2)$$

Generally speaking, the number density of electrons can be calculated as follows:

$$n_e(x) = \int_{-\infty}^{\infty} dv_{ex} \int_{-\infty}^{\infty} dv_{ey} \int_{-\infty}^{\infty} dv_{ez} f(x,v_e). \quad (3)$$

Substituting Eq. (2) into Eq. (3) and integrating, one can arrive at an expression for the number density at all points in space in terms of the usual error function erf,

$$n_e(x) = n_e(x_m)\exp\left(\frac{\psi_m - \psi}{kT_E}\right) \times \begin{cases} 1 - \mathrm{erf}\left[\left(\frac{\psi_m - \psi}{kT_E}\right)^{1/2}\right], & x > x_m \\ 1 + \mathrm{erf}\left[\left(\frac{\psi_m - \psi}{kT_E}\right)^{1/2}\right], & x_x < x < x_m \\ 1 + \mathrm{erf}\left[\left(\frac{\psi_m - \psi}{kT_E}\right)^{1/2}\right] - 2\,\mathrm{erf}\left[\left(\frac{\psi_{EB} - \psi}{kT_E}\right)^{1/2}\right], & x < x_x \end{cases} . \quad (4)$$

Again, this equation is valid between the emitter and collector; $x=0$ and $x=d$, respectively.

Poisson's equation can be written in terms of the motive as opposed to the electrostatic potential. In this case, it is given by

$$\frac{d^2\psi}{dx^2} = -\frac{e^2 n_e}{\epsilon_0}. \quad (5)$$

Substitution of Eq. (4) into Eq. (5) and a change in variables to dimensionless quantities yields the following dimensionless Poisson's equation:

$$2\frac{d^2\gamma}{d\xi^2} = \exp(\gamma) \times \begin{cases} 1 - \mathrm{erf}(\gamma^{1/2}), & \xi > 0 \\ 1 + \mathrm{erf}(\gamma^{1/2}), & \xi_x < \xi < 0, \\ 1 + \mathrm{erf}(\gamma^{1/2}) - 2\,\mathrm{erf}((\gamma - \theta_E)^{1/2}), & \xi < \xi_x, \end{cases} \quad (6)$$

where $\gamma \equiv (\psi_m - \psi)/kT_E$ is the dimensionless motive, $\xi \equiv (x - x_m)/x_0$ is the dimensionless distance, $x_0^2 \equiv (\epsilon_0 kT_E)/(2e^2 n_e(x_m))$ is a scaling factor to convert between dimensionless distance and actual distance, $\theta_E = (\psi_m - \psi_{EB})/kT_E$, and the initial conditions are $\gamma(0)=0$ and $\gamma'(0)=0$. Note that the dimensionless Poisson's equation given by Eq. (6) is parametrized by θ_E (Fig. 3). At the transition point x_x between regions ii and iii shown in Fig. 2(c) both the motive and first derivative of the motive are continuous.

Now the value of the current density must be determined. The current density is determined by the number of electrons traveling toward the collector at the point of maximum motive. This value is given by the following integral:

$$J = e\int_0^\infty dv_{ex}\int_{-\infty}^\infty dv_{ey}\int_{-\infty}^\infty dv_{ez} v_{ex} f(x_m, v_e). \quad (7)$$

Substituting Eq. (2) into Eq. (7) and integrating yields a manageable expression for current,

$$J = 2en_e(x_m)\left(\frac{kT_E}{2\pi m_e}\right)^{1/2}. \quad (8)$$

This J can be related to J_{ES} as follows: the electrons with thermal energy sufficient for emission from the emitter material. The saturation current is given by Richardson's equation: $J_{ES} = AT_E^2 \exp(-\zeta_E/kT_E)$. Additionally, the emitter saturation current can be calculated by evaluating Eq. (7) at the emitter, $x=0$,

$$J_{ES} = e\int_0^\infty dv_{ex}\int_{-\infty}^\infty dv_{ey}\int_{-\infty}^\infty dv_{ez} v_{ex} f(0, v_e). \quad (9)$$

Substituting the distribution function, Eq. (2), into Eq. (9), integrating, and combining the result with Eq. (8), one can obtain the following relation between the emitter saturation current and the output current of the device:

$$J = J_{ES}\exp(-\theta_E). \quad (10)$$

This result is sensible because the value θ_E quantifies the space charge barrier height above the barrier height of the emitter material. The output current of the TEC is thus decreased by the additional space charge barrier.

At this point, we are prepared to calculate the values of voltage and current density at the critical point, which is a matter of finding the proper value of θ_E for a particular output voltage. The following iterative procedure is used.

(1) Choose a value of $\theta_E \in [0, \theta_{E,\max}]$. The procedure to calculate $\theta_{E,\max}$ is discussed in part A of the appendix.
(2) Using the parameter θ_E, calculate the dimensionless motive from the dimensionless Poisson's equation given by Eq. (6).
(3) Calculate

$$\xi_E = -d\left(\frac{2\pi m_e e^2}{\epsilon_0^2 k^3}\right)^{1/4}\frac{J_{ES}^{1/2}}{T_E^{3/4}}\exp\left(-\frac{\theta_E}{2}\right). \quad (11)$$

(4) Use the ξ_E from step 3 as well as the dimensionless motive found in step 2 to calculate γ_E; the value of γ_E calculated from steps 2–4 will be denoted as $\gamma_{E,1}$.
(5) According to Fig. 2(d), γ_E is given by Eq. (12). Calculate this value, denoted as $\gamma_{E,2}$,

$$\gamma_{E,2} = \frac{\chi_E^-}{kT_E} + \theta_E. \quad (12)$$

(6) Compare the values of $\gamma_{E,1}$ and $\gamma_{E,2}$. Iterate by choosing different values of θ_E until $\gamma_{E,1}$ coincides with $\gamma_{E,2}$. The value of θ_E found in this way is denoted as θ_{ER}.
(7) Calculate the output current density at the critical point by substituting the value of θ_{ER} obtained above into Eq. (10). According to Fig. 2(d), the output voltage at the critical point, V_R, is given by

$$V_R = \frac{kT_E\theta_{ER} + \zeta_E - \phi_C}{e}. \quad (13)$$

A special case of the critical point algorithm is addressed in part B of the appendix.

B. Space charge limited output current characteristic

Once the virtual saturation point and critical point are known, the space charge limited output current characteristic is calculated by first specifying a value of current falling within the space charge limited regime, and then determining the corresponding output voltage.

Executing the following algorithm yields the space charge limited output current characteristic.

(1) Choose an intermediate value of current density $J \in (J_{VS}, J_R)$.
(2) Calculate the value of θ_E using Eq. (10).
(3) Using θ_E as the parameter, calculate the dimensionless motive by solving Eq. (6).
(4) Calculate γ_E using Eq. (12).
(5) Calculate ξ_E from γ_E using the dimensionless motive found in step 3.
(6) Calculate ξ_C

$$\xi_C = d\left(\frac{2\pi m_e e^2}{\epsilon_0^2 k^3}\right)^{1/4} \frac{J^{1/2}}{T_E^{3/4}} + \xi_E. \quad (14)$$

(7) Calculate γ_C from ξ_C using the dimensionless motive found in step 3.
(8) According to Fig. 2(c), the output voltage is given by

$$V = \frac{kT_E(\theta_E - \gamma_C) + \zeta_E - \phi_C}{e}. \quad (15)$$

III. RESULTS AND DISCUSSION

The theory presented in this report was implemented as a computer program in MATLAB. A TEC with a nitrogen doped diamond (NDD) emitter electrode was modeled. The emitter temperature was taken to be 950 K and the collector was taken to be 300 K. The barrier height of the NDD was considered to be 1.4 eV, and the collector barrier height was taken to be 0.6 eV. The emitter was considered to have a negative electron affinity of 0.5 eV. The emissivity of both the emitter and collector were taken to be 0.5. The interelectrode spacing was 10 μm in the calculations, and initially the Richardson's constant of both electrodes was assumed to be equal to the theoretical value of 120 A cm^{-2} K^{-2}.

Efficiency of these devices can be estimated by considering heat transport via the thermionic electrons $[Q_E = J(\psi_m - \mu_E + 2kT_E)/e]$ and Stefan–Boltzmann losses from the electrodes $[Q_r = \sigma_0(\epsilon_E T_E^4 - \epsilon_C T_C^4)]$, according to Hatsopoulous and Gyftopoulos[5] where ϵ_E and ϵ_C are the emissivities of the emitter and collector, respectively. The efficiency is given by

$$\eta = \frac{JV}{Q_E + Q_r}. \quad (16)$$

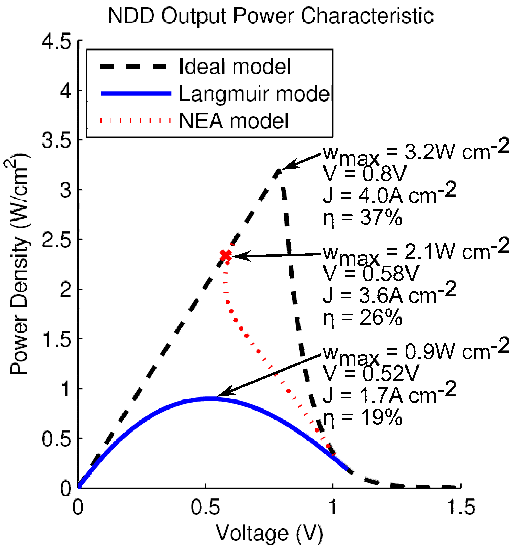

FIG. 4. (Color online) Output power characteristics of nitrogen doped diamond for the following set of parameters: T_E=950 K, A_E=120 A cm^{-2} K^{-2}, ζ_E=1.4 eV, χ_E=0.5 eV, ϵ_E=0.5, T_C=300 K, A_C=120 A cm^{-2} K^{-2}, ϕ_C=0.6 eV, ϵ_C=0.5, d=10 μm.

Using this set of parameters, the output power characteristics of the ideal model, the Langmuir model, and the NEA model were calculated and are compared in Fig. 4. The maximum output power of the ideal model is 3.2 W cm^{-2} with an efficiency of 37% and occurs at the contact potential of 0.8 V. The NEA model maximum output power is 2.3* W cm^{-2} with an efficiency of 27*% and occurs at the virtual saturation point voltage of 0.58* V, where the asterisk indicates this value is the physically realized value and noting that the output current characteristic in this case is not single valued. The maximum output power of the Langmuir model is 0.90 W cm^{-2}, its efficiency is 19% and occurs at voltage of 0.52 V. The maximum efficiency of the Langmuir model is 20.9% at an output power of 0.84 W cm^{-2} and occurs at a voltage of 0.66 V. The carnot efficiency of a device operating between these temperatures is 68%. These data show that a TEC with a NEA emitter outperforms a TEC with a conventional emitter in terms of output power and efficiency because the NEA property mitigates the negative space charge effect.

In reality, thermionic materials have Richardson's constants less than the theoretical maximum value. Consider a TEC with the same parameters as before, but with a Richardson constant of 10 A cm^{-2} K^{-2} for both electrodes. The resulting output power characteristics from the ideal, NEA, and Langmuir models are shown in Fig. 5. The maximum output power of the ideal and NEA case is 0.27 W cm^{-2} at an efficiency of 9.5% occurring at the contact potential of 0.8 V. The maximum output power of the Langmuir model is 0.23 W cm^{-2} at an efficiency of 8.1% occurring at a voltage of 0.70 V. In this scenario, the NEA device meets the special case conditions, and therefore it has an output current characteristic identical to that of the ideal case. In fact, the minimum value of χ_E for this TEC to meet the special case condition is 0.14 eV. Furthermore, the Langmuir model ex-

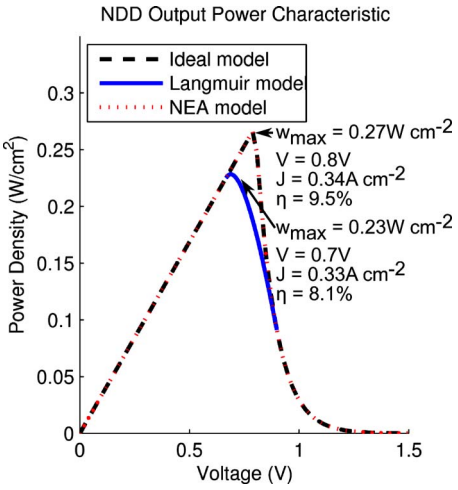

FIG. 5. (Color online) Output power characteristics of nitrogen doped diamond for the following set of parameters: T_E=950 K, A_E=10 A cm^{-2} K^{-2}, ζ_E=1.4 eV, χ_E^-=0.5 eV, ϵ_E=0.5, T_C=300 K, A_C=10 A cm^{-2} K^{-2}, ϕ_C=0.6 eV, ϵ_C=0.5, d=10 μm.

hibits a much smaller space charge effect as a result of the reduction in output current due to a smaller Richardson's constant.

IV. CONCLUSIONS

In this report, a theory was developed to model the space charge limited electron transport across the interelectrode space of a vacuum thermionic energy conversion device employing a negative electron affinity emitter material. This theory was written in terms of algorithms which were implemented as computer programs in MATLAB. Two interesting mathematical consequences of the theory were introduced; namely, the nonsingle valued output current characteristic and the equivalence of the special case conditions of the virtual saturation point and critical point. Calculations were performed to model the performance of such a NEA TEC under reasonable conditions with a nitrogen doped diamond material as the emitter electrode.

In general, a vacuum TEC with a negative electron affinity emitter material will outperform a TEC with a conventional emitter material. The NEA property mitigates the negative space charge by lowering the electrostatic boundary condition just outside the emitter electrode, therefore improving the output power and efficiency of the device over the conventional device. The presence of NEA mathematically yields an output current characteristic which is not single valued, but a simple nonequilibrium thermodynamics argument yields a single-valued, physically plausible curve. Additionally, for a set of operating parameters, there exists a value of the NEA such that the TEC does not experience a space charge limited mode and therefore operates exactly like an ideal TEC.

Hydrogen terminated nitrogen doped diamond was considered as an emitter material in the calculations. For a Richardson's constant equal to the theoretical value, the NEA model outperformed the Langmuir model in terms of output power and efficiency at the maximum output power. Additionally, under these conditions, the output current characteristic was not single valued.

When a Richardson's constant of 10 A cm^{-2} K^{-2} was considered, the emitter saturation current was reduced and therefore the space charge effect was reduced. The NEA model will not experience a space charge limited mode for values of χ_E^-=0.14 eV and above.

From a theoretical standpoint, hydrogen terminated, doped diamond materials show unique promise as the emitter material of a vacuum TEC. These materials provide an approach to mitigate the performance degrading space charge limitation of the vacuum TEC without requiring submicron sized interelectrode spacings or plasmas.

ACKNOWLEDGMENT

This research was supported by the Office of Naval Research through the TEC MURI program.

APPENDIX: MATHEMATICAL ANALYSIS

We have collected several mathematical details in the appendix to present a more complete description of the theory and to avoid distracting the reader with these mathematical intricacies. In part A we provide arguments and derivations to describe the upper bound of θ_E in the critical point calculation. In part B we describe the special case condition of the critical point. In part C the nonsingle-valued nature of the output current characteristic is discussed. Finally, in part D we prove the equivalence of the virtual saturation point and critical point special case conditions.

1. CRITICAL POINT: UPPER BOUND OF θ_E

For a set of device parameters, there exists an upper bound on the value of θ_E, denoted as $\theta_{E,\max}$. This upper bound exists as a result of the following restriction: the position of the emitter is strictly less than the position of x_x. The value of $\theta_{E,\max}$ is essentially the condition which forces the emitter position and x_x to be coincident.

This issue is most easily approached in the space of the dimensionless motive and dimensionless distance. The crux of this argument is that the value of ξ_E is strictly less than the value of ξ_x. The value of $\theta_{E,\max}$ is the value which results in the condition $\xi_E=\xi_x$. Both ξ_E and ξ_x can be calculated given a value of θ_E. For ξ_x, consider the following.

- The dimensionless Poisson's equation, Eq. (6), is identical to Langmuir's dimensionless Poisson's equation in regions i and ii, as are the initial conditions. Therefore, the solution of both equations is identical in those regions.
- The point ξ_x is the boundary between regions ii and iii.
- The point ξ_x corresponds to the value of θ_E on the solution to Eq. (6).
- At the point ξ_x, the motive and its first derivative are continuous.

As a result, the point on the solution to Eq. (6) corresponding to ξ_x is coincident with the point on Langmuir's curve. Thus, it is established that ξ_x and θ_E are related via the solution to

Langmuir's dimensionless Poisson's equation. Additionally, the reader will note that ξ_E is related to θ_E by Eq. (11). The lower bound on θ_E is clearly zero. As θ_E increases, ξ_x becomes more negative, approaching the asymptote of Langmuir's dimensionless Poisson's equation, while ξ_E becomes less negative, approaching zero. Thus, to satisfy $\xi_E < \xi_x$, the upper bound on θ_E is given by the intersection of the two curves.

There exists a special case of the critical point algorithm with physical consequences. The derivation of this special case can be found in part B of the appendix, and the physical consequences will be discussed in Sec. III.

2. CRITICAL POINT: SPECIAL CASE

In the space charge limited regime there exists two independent ways to calculate the value of γ_E. A special case of the critical point algorithm exists when there is no value of θ_E such that these two methods yield the same value of γ_E. The special case occurs when the following condition is met:

$$\frac{\chi_E^-}{kT_E} > \gamma_{\theta_E=0}\left[-d\left(\frac{2\pi m_e e^2}{\epsilon_0^2 k^3}\right)^{1/4}\frac{J_{ES}^{1/2}}{T_E^{3/4}}\right], \tag{A1}$$

where $\gamma_{\theta_E=0}$ is the solution to Eq. (6) calculated for $\theta_E=0$. As a result of this special case condition, the output voltage and output current are given by the contact potential ($V_{CP} \equiv \phi_E - \phi_C$) and saturation current density, respectively. In the following discussion, we derive the critical point special case condition.

The two independent methods used to calculate the value of γ_E are articulated in the critical point algorithm found in Sec. II A. One way to calculate the value of γ_E is given in steps 2–4 of the algorithm and is denoted by $\gamma_{E,1}$. The second method is given in step 5 of the algorithm and is denoted $\gamma_{E,2}$. Both $\gamma_{E,1}$ and $\gamma_{E,2}$ are continuous functions of their variables and both depend on the value of θ_E. It has been shown in part A of the appendix that legitimate values of θ_E are bounded above and below. If the difference $\gamma_{E,1}-\gamma_{E,2}$ does not change sign when evaluated at the bounds of θ_E, then the special case occurs because there is no value of θ_E such that $\gamma_{E,1}=\gamma_{E,2}$ or in other words $\gamma_{E,1}-\gamma_{E,2}=0$.

We quantify this scenario as follows: consider the bound $\theta_E=\theta_{E,\max}$. In this situation, the value of $\gamma_{E,1}$ will always be equal to $\theta_{E,\max}$. The value of $\gamma_{E,2}$ is given by

$$\gamma_{E,2} = \frac{\chi_E^-}{kT_E} + \theta_{E,\max}. \tag{A2}$$

Comparing,

$$\frac{\chi_E^-}{kT_E} + \theta_{E,\max} > \theta_{E,\max}, \tag{A3}$$

$$\gamma_{E,2} > \gamma_{E,1}. \tag{A4}$$

Note that the inequality in Eq. (A4) is a general result when $\theta_E=\theta_{E,\max}$. Therefore if the same inequality occurs for the bound $\theta_E=0$, the critical point special case occurs.

Next consider $\theta_E=0$. The value of $\gamma_{E,2}$ is given by

$$\gamma_{E,2} = \frac{\chi_E^-}{kT_E}. \tag{A5}$$

The value of ξ_E from step 3 of the critical point algorithm is given by

$$\xi_E = -d\left(\frac{2\pi m_e e^2}{\epsilon_0^2 k^3}\right)^{1/4}\frac{J_{ES}^{1/2}}{T_E^{3/4}}. \tag{A6}$$

The value of $\gamma_{E,1}$ is determined by substituting the result from Eq. (A6) into the solution to the dimensionless Poisson equation evaluated when $\theta_E=0$. The crux here is to notice that ξ_E in Eq. (A6) does not depend on the value of χ_E^- but $\gamma_{E,2}$ from Eq. (A5) does. Therefore, χ_E^- can be increased arbitrarily until the following inequality is satisfied,

$$\frac{\chi_E^-}{kT_E} > \gamma_{\theta_E=0}\left[-d\left(\frac{2\pi m_e e^2}{\epsilon_0^2 k^3}\right)^{1/4}\frac{J_{ES}^{1/2}}{T_E^{3/4}}\right], \tag{A7}$$

$$\gamma_{E,2} > \gamma_{E,1}. \tag{A8}$$

As a result, a value of χ_E^- can be chosen such that the previous inequality can be forced for both bounds of θ_E. In this special case, the output voltage and output current density are given by the contact potential ($V_{CP} \equiv \phi_E - \phi_C$) and saturation current density, respectively.

There remains the pathological possibility of several roots within the bounds. If so, an even number of roots would exist, but we have not encountered this case for the material parameters of the diamond emitter.

3. ON THE NONSINGLE-VALUED NATURE OF THE OUTPUT CURRENT CHARACTERISTIC

From Fig. 2, it is clear that the output current characteristic is not single valued for a certain set of voltages. For insight, consider the set of voltages for which the output current characteristic is not single valued. For a particular voltage, say V_0, there are three possible current states in which the system might exist; shown in Fig. 6(a) as J_a, J_b, and J_c. Each value of current is a mathematically legitimate value from an electrostatic perspective. Consider the motive diagram for each value of output current, shown in Fig. 6(b). For all three, the boundary conditions are the same. However, the differential equations for these boundary conditions are not. For J_a, the Poisson equation is given by

$$2\frac{d^2\gamma}{d\xi^2} = \exp(\gamma)[1-\mathrm{erf}(\gamma^{1/2})]. \tag{A9}$$

For J_b and J_c, the form of Poisson's equation is given by Eq. (6) but the parameter θ_E is different for both. Therefore, a unique differential equation exists for all three values of current. For this scenario, the key is not that each point has the same boundary conditions, it is that each case corresponds to a unique formulation of Poisson's equation. Therefore, each state is mathematically possible.

Despite the mathematical possibility of three unique output current states for a particular value of output voltage, the physical system will only select one state. It is conceivable

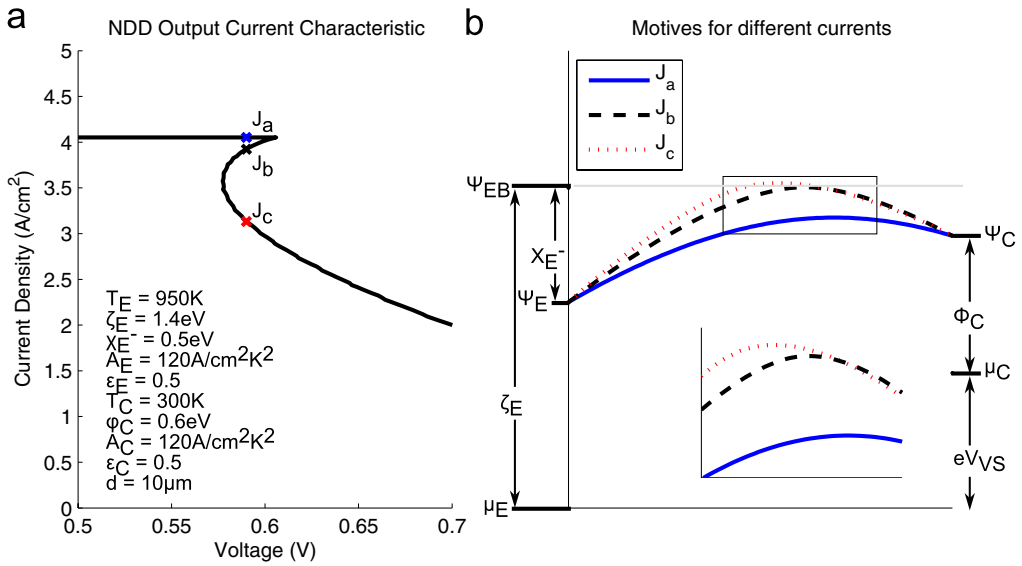

FIG. 6. (Color online) (a) Output current characteristic showing nonsingle valuedness. (b) Different motive diagrams for the same value of output current in the space charge limited mode for a NEA TEC. The dimensionless Poisson's equations are different for these motives. The inset shows an enlarged view of the different motives.

that the system will oscillate between states; indeed, this behavior has been reported in other types of TEC systems.[23] To fully address this problem, the electron transport theory would need to be derived using the time dependent Vlaslov equation which is unfortunately beyond the scope of this discussion. According to Prigogine's[24] work on nonequilibrium thermodynamics, a nonequilibrium system in a stationary state is characterized by the state the that produces the minimum entropy. Thus,

$$\dot{S} = \frac{\dot{Q}}{T} = \frac{P}{T}. \tag{A10}$$

To minimize this expression, the system will select the branch corresponding to the minimum output power.

The algorithm and program which produce the output current characteristic give the entire curve. The branch associated with the accelerating regime is given by the saturation current of the emitter up to the virtual saturation points and the determination of this branch is independent of the determination of any other branch. For the space charge limited regime, the curve is determined by considering the output current density as the independent variable and calculating the corresponding output voltage, in which case the result is single valued. When the entire output current characteristic is finally assembled by the program, all of the mathematically possible states are given.

4. EQUIVALENCE OF THE VIRTUAL SATURATION POINT AND CRITICAL POINT SPECIAL CASES

According to the theory of the virtual saturation point,[1] there exists a special case of the virtual saturation point; therefore the output current and output voltage are equal to the saturation current and contact potential, respectively. The virtual saturation point special case and the critical point special case are equivalent: the conditions resulting in one will result in the other. To demonstrate this claim it will be shown that for a given set of parameters, a special minimum value of χ_E^- exists for which both special cases occur. For values of χ_E^- greater than this special value, both special cases occur. For values of χ_E^- less than this special value, neither special case occurs, and the device behaves according to the theory described in this paper. The derivation unfolds as follows: first, a minimum value of NEA, $\xi_{E,1}^-$, is established such that the virtual saturation point special case occurs. Next, a minimum value of NEA, $\xi_{E,2}^-$, is established such that the critical point special case occurs. Finally, it is shown that $\xi_{E,1}^- = \xi_{E,2}^-$.

First, recalling the discussion from Ref. 1 consider the special case condition of the virtual saturation point,

$$-\xi_E \left(\frac{\epsilon_0^2 k^3}{2\pi m_e e^2} \right)^{1/4} \frac{T_E^{3/4}}{J_{ES}^{1/2}} \geqslant d. \tag{A11}$$

Here, the value of χ_E^- determines the value of γ_E, which in turn determines the value of ξ_E. Each relationship is monotonic. Therefore, there exists a unique value of χ_E^-, referred to as $\chi_{E,1}^-$, such that the equality in Eq. (A11) holds. For values of $\chi_E^- < \chi_{E,1}^-$ the virtual saturation point special case does not occur because the condition in Eq. (A11) is not met. For values of $\chi_E^- > \chi_{E,1}^-$, the virtual saturation point occurs by definition.

Next, consider the critical point special case. This situation occurs when the following condition is met:

$$\gamma_{E,2} \geqslant \gamma_{E,1}, \theta_E = 0, \tag{A12}$$

where the reader will recall from part B of the appendix the definitions of $\gamma_{E,2}$ and $\gamma_{E,1}$. Note that the value of $\gamma_{E,1}$ does not depend on the value of χ_E^-, but the value of $\gamma_{E,2}$ does.

Moreover, the value of $\gamma_{E,2}$ depends monotonically on the value of χ_E^-. Therefore, there exists a minimum value of χ_E^-, referred to as $\chi_{E,2}^-$, such that the equality in Eq. (A12) is satisfied. For values of $\chi_E^- < \chi_{E,2}^-$, the inequality is not satisfied and the critical point special case does not occur. For $\chi_E^- > \chi_{E,2}^-$, the inequality is satisfied and the critical point special case occurs by definition. At this point, it has been shown that there exists minimum values of χ_E^- for each special case such that each occurs.

The next step is to show that those values are equal. Consider the virtual saturation point algorithm when $\chi_E^- = \chi_{E,1}^-$. In the first step, the value of γ_E is calculated,

$$\gamma_{E,V} = \frac{\chi_{E,1}^-}{kT_E}. \tag{A13}$$

Next, the solution to Eq. (A9) is used to determine the corresponding value of ξ_E, denoted here as $\xi_{E,V}$. Finally, since $\chi_E^- = \chi_{E,1}^-$, the equality from Eq. (A11) holds,

$$-\xi_{E,V}\left(\frac{\epsilon_0^2 k^3}{2\pi m_e e^2}\right)^{1/4} \frac{T_E^{3/4}}{J_{ES}^{1/2}} = d. \tag{A14}$$

Next, consider the critical point algorithm when $\chi_E^- = \chi_{E,2}^-$. In this situation, the critical point condition is met when $\theta_E = 0$. Thus, the critical point value of ξ_E (denoted by $\xi_{E,R}$) determined by Eq. (11) is given by

$$\xi_{E,R} = -d\left(\frac{2\pi m_e e^2}{\epsilon_0^2 k^3}\right)^{1/4} \frac{J_{ES}^{1/2}}{T_E^{3/4}}. \tag{A15}$$

Notice that this expression can be rearranged to yield Eq. (A14). Therefore, $\xi_{E,R} = \xi_{E,V}$. Since $\chi_E^- = \chi_{E,2}^-$, the equality in Eq. (A12) holds. Since $\theta_E = 0$, the critical point dimensionless Poisson's equation given by Eq. (6) is equal to the virtual saturation point Poisson's equation given by Eq. (A9) and so the solutions to both will be equal. As a result, the value of γ_E (referred to as $\gamma_{E,R}$) corresponding to $\xi_{E,R}$ will be

$$\gamma_{E,R} = \gamma_{E,V} \tag{A16}$$

Recalling Eq. (A12), Eq. (12) can be substituted in for $\gamma_{E,2}$ with the condition $\theta_E = 0$ yielding

$$\frac{\chi_{E,2}^-}{kT_E} = \gamma_{E,V}. \tag{A17}$$

Substituting Eq. (A13), one has

$$\chi_{E,2}^- = \chi_{E,1}^-. \tag{A18}$$

Therefore it has been shown that the virtual saturation point special case and critical point special case are equivalent. The major result is as follows: in the event of the special case, the virtual saturation point and the critical point occur coincident with the contact potential point on the output current characteristic of the ideal model. Thus, the NEA device operating in the condition given by Eq. (A11) does not exhibit a space charge limited mode in the sense that it performs identically to an ideal device.

[1] J. R. Smith, G. Bilbro, and R. Nemanich, Phys. Rev. B **76**, 245327 (2007).
[2] W. Schlichter, Ann. Phys. **47**, 573 (1915).
[3] J. M. Houston, J. Appl. Phys. **30**, 481 (1959).
[4] H. Moss, J. Electron. Control **2**, 305 (1957).
[5] G. N. Hatsopoulous and E. P. Gyftopoulos, *Thermionic Energy Conversion* (MIT Press, Cambridge, MA, 1973), Vol. 1.
[6] F. J. Himpsel, J. A. Knapp, J. A. VanVechten, and D. E. Eastman, Phys. Rev. B **20**, 624 (1979).
[7] C. Bandis and B. B. Pate, Phys. Rev. B **52**, 12056 (1995).
[8] J. van der Weide, Z. Zhang, P. K. Baumann, M. G. Wensell, J. Bernholc, and R. J. Nemanich, Phys. Rev. B **50**, 5803 (1994).
[9] L. Diederich, O. M. Küttel, E. Schaller, and L. Schlapbach, Surf. Sci. **349**, 176 (1996).
[10] P. K. Baumann and R. J. Nemanich, Surf. Sci. **409**, 320 (1998).
[11] P. A. L. Diederich, O. M. Küttel, and L. Schlapbach, Surf. Sci. **418**, 219 (1998).
[12] I. L. Krainsky, V. M. Asnin, G. T. Mearini, and J. A. Dayton, Phys. Rev. B **53**, R7650 (1996).
[13] R. G. Farrer, Solid State Commun. **7**, 685 (1969).
[14] S. Koizumi, Phys. Status Solidi A **172**, 71 (1999).
[15] S. Koizumi, T. Teraji, and H. Kanda, Diamond Relat. Mater. **9**, 935 (2000).
[16] Y. Tang, Ph.D. thesis, North Carolina State University, 2007.
[17] F. A. M. Koeck and R. J. Nemanich, Diamond Relat. Mater. **15**, 217 (2006).
[18] J. R. Smith, G. L. Bilbro, and R. J. Nemanich, Diamond Relat. Mater. **15**, 2082 (2006).
[19] G. N. Hatsopoulous and E. P. Gyftopoulos, *Thermionic Energy Conversion* (MIT Press, Cambridge, MA, 1979), Vol. 2.
[20] A. F. Dugan, J. Appl. Phys. **31**, 1397 (1960).
[21] J. R. Smith, R. J. Nemanich, and G. L. Bilbro, Diamond Relat. Mater. **15**, 870 (2006).
[22] I. Langmuir, Phys. Rev. **21**, 419 (1923).
[23] P. Burger, J. Appl. Phys. **36**, 1938 (1965).
[24] I. Prigogine, *Introduction to Thermodynamics of Irreversible Processes*, 2nd ed. (InterScience, New York, 1961).